

# A meshless approach towards solution of macrosegregation phenomena

Gregor Kosec<sup>1</sup>, Miha Založnik<sup>2</sup>, Božidar Šarler<sup>1</sup> and Hervé Combeau<sup>2</sup>

**Abstract** The simulation of macrosegregation as a consequence of solidification of a binary Al-4.5%Cu alloy in a 2-dimensional rectangular enclosure is tackled in the present paper. Coupled volume averaged governing equations for mass, energy, momentum and species transfer are considered. The phase properties are resolved from the Lever solidification rule, the mushy zone is modeled by the Darcy law and the liquid phase is assumed to behave like an incompressible Newtonian fluid. Double diffusive effects in the melt are modeled by the thermal and solutal Boussinesq hypothesis. The physical model is solved by the novel Local Radial Basis Function Collocation Method (LRBFCM). The involved physical relevant fields are represented on overlapping 5-noded sub-domains through collocation by using multiquadrics Radial Basis Functions (RBF). The involved first and second derivatives of the fields are calculated from the respective derivatives of the RBFs. The fields are solved through explicit time stepping. The pressure-velocity coupling is calculated through a local pressure correction scheme. The evolution of the solidification process is presented through temperature, velocity, liquid fraction and species concentration histories in four sampling points. The fully solidified state is analyzed through final macrosegregation map in three vertical and three horizontal cross-sections. The results are compared with the classical Finite Volume Method (FVM). A surprisingly good agreement of the numerical solution of both methods is shown and therefore the results can be used as a reference for future verification studies. The advantages of the represented meshless approach are its simplicity, accuracy, similar coding in 2D and 3D, and straightforward applicability in non-uniform node arrangements. The paper probably for the first time shows an application of a meshless method in such a highly non-linear and multi-physics problem.

**Keywords:** Solidification, binary alloy, macrosegregation, convective-diffusive problems, meshless method, local radial basis function collocation method, finite volume method.

## 1 Introduction

Solidification processing is increasingly transforming from art to science based on the extensive use of multi-scale and multi-physics numerical models [Cockcroft and Maijer, (2009)]. These models are becoming increasingly important in technology, because they help to understand a broad spectra of solidification situations, such as casting, crystal growth, welding, etc. On the other hand, they help to mitigate several casting defects such as macrosegregation, cracks, shape defects, porosity, hot tearing, etc. The present work deals with the numerical prediction of macrosegregation in cast pieces. Macrosegregation is an inhomogeneity of the chemical composition in a cast piece that forms during the solidification process as a consequence of coupled heat and mass transfer, phase change and flow phenomena. The theoretical description of this phenomenon started to attract researchers in the Sixties [Flemings and Nereo, (1967a); Flemings and Nereo, (1967b)] and model studies started in the Seventies [Hebditch and Hunt, (1974)]. Since then, this topics has been treated in many theoretical works and for many processes such as static casting [Combeau, Založnik, Hans and Richey, (2009); Založnik, Kumar and Combeau, (2010)], continuous casting of steel [Lesoult, (2005)] and direct chill casting of aluminum alloys [Založnik and Šarler, (2005)]. Despite the many different attempts by using different formulations of the physical system [Drew, (1983); Ganesan and Poirier, (1990); Ni and Beckermann, (1991); Wang and Beckermann, (1996a); Wang and Beckermann, (1996b); Goyeau, Bousquet-Melou, Gobin, Quintard and Fichot, (2004)] and different numerical methods [Ahmad, Combeau, Desbiolles, Jalanti, Lesoult, Rappaz, Rappaz and Stomp, (1998)], it is still very difficult to obtain accurate numerical predictions of macrosegregation, which would be independent of the spatial discretization or even of the numerical method. Only recently substantial efforts were invested to study [Combeau, Bellet, Fautrelle, Gobin, Arquis, Budenkova, Dussoubs, Duterrail, Kumar, Goyeau, Mosba, Quatruvaux, Rady, Gandin and Založnik, (2011)] the behavior of different numerical meth-

<sup>1</sup>University of Nova Gorica

Vipavska 13, SI-5000 Nova Gorica, Slovenia

gregor.kosec@ung.si, bozidar.sarler@ung.si, www.ung.si

<sup>2</sup>Institut Jean Lamour, CNRS – Nancy-Université – UPV Metz

Ecole des Mines de Nancy, Parc de Saurupt CS14234, F-54042 Nancy cedex, France

miha.zaloznik@mines.inpl-nancy.fr, herve.combeau@ijl.nancy-universite.fr, www.ijl.nancy-universite.fr

ods in the prediction of macrosegregation. However, these studies were made on numerical benchmark test cases, where instabilities develop during solidification that induce fine scale segregation structures (also called mesosegregations). These structures are very difficult to resolve because they require extremely fine spatial discretizations and because their development is strongly nonlinear. Due to this high complexity, grid independent solutions could not be obtained until now. In summary, today we do still not have a rigorous and clear-cut view of the convergence behavior and the precision of numerical methods in the prediction of macrosegregation.

The simulation of a numerical test case for macrosegregation that is similar to the one proposed in [Bellet, Combeau, Fautrelle, Gobin, Rady, Arquis, Budenkova, Dussoubs, Duterrail, Kumar, Gandin, Goyeau, Mosbah and Založnik, (2009)], however without the appearance of the fine mesosegregation structures in the solution, is treated in the present paper. There are two basic incitements for doing this. The first one is in solving the highly nonlinear macrosegregation problem by a new generation of meshless numerical methods, which can be generally very well suited for moving boundary problems. The second one is to propose a simpler test case for macrosegregation and show that we could be able to find an accurate numerical reference solution for such a case. We demonstrate this by solving the problem with two completely different methods: a novel local meshless method and a classical FVM for spatial discretization, with different time discretization schemes, and different pressure velocity couplings. Both of the two topics have, by the best of the knowledge of the present authors, not been published yet.

The meshless numerical methods represent one of the most vigorously developing fields of numerical mathematics and engineering. They are characterized by involvement of the nodal points only, instead of polygons. This usually makes these methods attractive in three dimensional situations, node refinement situations, and in complex geometry cases with moving boundaries. Undoubtedly, these methods can be of great advantage in solving solidification processing problems. There are many different meshless methods in development today. Some of them are based on the weak formulation and some of them on the strong one. There is a particularly simple and appealing class of meshless methods, based on the strong formulation and collocation by radial basis functions [Buhmann, (2000)]. This development was initiated by the pioneering work of Kansa [Kansa, (1990b); Kansa, (1990a)]. His idea was to solve the partial differential equations by collocation of the involved fields in a global sense with radial basis functions (RBFs). The partial differential operators have been calculated through partial derivatives of the RBFs. This procedure has been used for solving many different partial differential equations. However, the procedure

resulted in large, increasingly ill-conditioned systems of equations, which prevented the problems with more than approx. 1000 variables to be solved in a reliable way. Šarler and Vertnik proposed [Šarler and Vertnik, (2006)] a local variant of this method, where the collocation is done locally over a subset (usually 5 nodes in 2 dimensions). This procedure results in small systems of collocation equations for each node, which are less sensitive to the free parameters of RBFs. The method experienced extremely fast and successful development, by recently being applied even to simulations of turbulent flow in channels [Vertnik and Šarler, (2009)] and turbulent mixed convection [Vertnik and Šarler (2011)]. Lee et al. [Lee, Liu and Fan, (2003)] show that the method is approximately of the same accuracy as the global one for a spectrum of boundary value problems tested. In order to be able to simulate the posed problem of this paper, the method previously needed to be developed for convective-diffusive problems with phase change [Vertnik and Šarler, (2006)], thermal and solutal natural convection problems in Newtonian fluids [Kosec and Šarler, (2008a)], natural convection problem in Darcy porous media [Kosec and Šarler, (2008b)] and natural convection with melting of a pure metal [Kosec and Šarler, (2008c); Kosec and Šarler, (2009)]. The next step in the order of increasing complexity is represented by the present problem – solidification of a binary alloy.

The main complexities in solving physical models of alloy solidification are strong nonlinearities and strong couplings. The nonlinearities stem from the hyperbolic nature of the solute transport (completely advective transport) in the potentially unstable natural convection in low-Pr liquids such as metals, in the jump of the enthalpy in the mushy zone and in the two flow regimes in free fluid and in the flow resistant mushy zone. On the other hand, the problem of strong coupling between the momentum transport and energy and solute transport via buoyancy force, and between the thermal field and permeability, makes the solution even less stable. The complexity of the prediction of macrosegregation is a consequence of the fact that the macrosegregation results from the entire history of the strongly coupled processes of mass, heat, momentum and solute transfer from the liquid state up to the end of solidification. Recent results of a numerical benchmark, proposed within the French SMACS [Bellet, Combeau, Fautrelle, Gobin, Rady, Arquis, Budenkova, Dussoubs, Duterrail, Kumar, Gandin, Goyeau, Mosbah and Založnik, (2009)] project, have shown the difficulties in the numerical solution of the macrosegregation problem, mainly linked to the presence of mesosegregates, i.e. instabilities that developed into channels during the advancement of the mushy zone, and which make the problem even more unpredictable. The results also show that the predictions of macrosegregation (outside the instability zone) are seemingly an easier problem, despite the apparent nonlinearities involved. Additional research is needed to understand all of the involved phenomena and their interactions.

## 2 Problem definition

The physical model used to describe the macrosegregation in the present paper is based on continuum Euler description of the conservation laws and constitutive relations, contributing additional information regarding the diffusion transport, stresses, interfacial forces, buoyancy forces,... The governing equations presented in this paper are derived by the volume averaging procedure. The original derivation of the model can be found in the paper of Ni and Beckerman [Ni and Beckermann, (1991)] as well as in the follow-up papers [Drew, (1983); Ganesan and Poirier, (1990); Wang and Beckermann, (1996a); Wang and Beckermann, (1996b)] and later developments in the field [Goyeau, Bousquet-Melou, Gobin, Quintard and Fichot, (2004)]. To avoid the two-domain formulation, which includes the phase change front tracking with the boundary conditions on the phase change front, a one-domain model is developed. In the first step, the transport equations for each phase are averaged separately and then summed up by taking into account the interphase balances. On the microscopic level, the phase change phenomena are treated by the consideration of the linearized phase diagram and solute transport over the scale of the secondary dendritic arms [Flemings, (1974); Voller, (2001)]. Essentially, this paper deals with the same physical model as in the French SMACS [Bellet, Combeau, Fautrelle, Gobin, Rady, Arquis, Budenkova, Dussoubs, Duterrail, Kumar, Gandin, Goyeau, Mosbah and Zaloznik, (2009)] project, but with material and process conditions, where no headache with the channel mesosegregations is expected. A first comparison of channel mesosegregation predictions, obtained by the finite volume and the finite element method, has been attempted in [Ahmad, Combeau, Desbiolles, Jalanti, Lesoult, Rappaz, Rappaz and Stomp, (1998)] and it has been found out that the mesosegregates are more pronounced when calculated by the FVM. Unfortunately, a comparison of mesosegregation-free case, such as the one in the present paper, have not been attempted before.

A columnar solidification process in two-dimensional rectangular domain  $\Omega$  with boundary  $\Gamma$ , filled with a binary substance in solid and liquid phase, is considered. The simplest possible description that can provide physically reasonable predictions, a so-called “minimal” (simplified to the largest possible degree) solidification model, is considered for the defined system. At the macroscopic scale it accounts for heat transfer, solute transport and for incompressible Newtonian flow, driven by thermosolutal natural convection. The Boussinesq hypothesis is used to describe the buoyancy force. The solidification region (mushy zone) is a developing columnar grain structure with interconnected solid phase. At the macroscopic scale it is described as a porous medium, which exerts a Darcy drag on the moving fluid. The phase change is modeled assuming local thermodynamic equilibrium (Lever rule) at the scale of the solidification structures (microscopic scale – the scale of the grains or dendrites) and is fully cou-

pled with the macroscopic transport. The problem is described by the following system of partial differential equations, identical as proposed in [Bellet, Combeau, Fautrelle, Gobin, Rady, Arquis, Budenkova, Dussoubs, Duterrail, Kumar, Gandin, Goyeau, Mosbah and Zaloznik, (2009)].

$$\nabla \cdot \mathbf{v} = 0, \quad (1)$$

$$\rho \frac{\partial \mathbf{v}}{\partial t} + \frac{\rho}{f_L} (\nabla \mathbf{v}) \mathbf{v} = -f_L \nabla P + \mu \nabla^2 \mathbf{v} - f_L \frac{\mu}{K} \mathbf{v} + f_L \mathbf{b}, \quad (2)$$

$$\rho \frac{\partial h}{\partial t} + \rho \mathbf{v} \cdot \nabla h = \lambda \nabla^2 T, \quad (3)$$

$$\frac{\partial C}{\partial t} + \mathbf{v} \cdot \nabla C_L = 0; \quad (4)$$

$$\mathbf{v} = f_L \mathbf{v}_L, \quad (5)$$

$$K = K_0 \frac{f_L^3}{(1-f_L)^2}, \quad (6)$$

$$\mathbf{b} = \rho_{\text{ref}} [1 - \beta_T (T - T_{\text{ref}}) - \beta_C (C_L - C_{\text{ref}})] \mathbf{g}, \quad (7)$$

$$h = c_p T + f_L L, \quad (8)$$

$$C = [f_L + (1-f_L)k_p] C_L, \quad (9)$$

$$T = T_F + m C_L, \quad (10)$$

The transport equations (5)-(4) describe the temporal evolution of the leading quantities,  $\mathbf{v}, h, C$ : superficial liquid velocity, enthalpy, and average concentration, respectively, as well as the pressure  $P$ .  $\mathbf{v}_L$  stands for the intrinsic liquid velocity. The permeability  $K$  is linked to a permeability constant  $K_0$  and to the liquid fraction  $f_L$  by the Kozeny-Carman relation (6). The thermal conductivity  $\lambda$ , specific heat  $c_p$  and density  $\rho$  of the solid and the liquid phase are assumed to be equal and constant. The liquid density varies only in the buoyancy term  $\mathbf{b}$  (Boussinesq hypothesis), where it depends on the temperature  $T$ , the liquid concentration  $C_L$ , the thermal expansion coefficient  $\beta_T$ , the concentration expansion coefficient  $\beta_C$ , as well as on the reference density  $\rho_{\text{ref}}$  given at reference temperature  $T_{\text{ref}}$  and reference concentration  $C_{\text{ref}}$ . The viscosity  $\mu$ , the liquidus slope  $m_L$  and the binary equilibrium partition coefficient  $k_p$ , are constant as well. The symbols  $t, \mathbf{g}, T_F$  stand for time, gravity acceleration and the fusion temperature of the pure solvent, respectively. The solute diffusion is neglected at the macroscopic scale.

We seek the solution of the enthalpy, velocity, pressure and concentration field at time  $t = t_0 + \Delta t$ , where  $t_0$  represents initial time and  $\Delta t$  a positive time increment. We solve the transport equations (1)-(5) by integration in time. They are coupled to the equations (8)-(10), which describe the phase

change. They are solved to get the additional variables  $f_L$ ,  $T$ , and  $C_L$ .

The initial and boundary conditions on the considered rectangle are set to

$$\mathbf{v}(p_x = \Omega_w, t) = \mathbf{v}(p_y = \Omega_H, t) = \mathbf{v}(p_y = 0, t) = 0, \quad (11)$$

$$\frac{\partial}{\partial p_x} v_y(p_x = 0, t) = 0, \quad v_x(p_x = 0, t) = 0, \quad (12)$$

$$\frac{\partial}{\partial p_x} T(p_x = \Omega_w, t) = \frac{q}{\lambda}(T - T_{ext}), \quad (13)$$

$$\frac{\partial}{\partial p_x} T(p_x = 0, t) = \frac{\partial}{\partial p_y} T(p_y = 0, t) = \frac{\partial}{\partial p_y} T(p_y = \Omega_H, t) = 0 \quad (14)$$

$$\frac{\partial}{\partial p_x} C(p_x = 0, t) = 0, \quad (15)$$

$$C(p_x = \Omega_w, t) = C(p_y = \Omega_H, t) = C(p_y = 0, t) = C_0, \quad (16)$$

$$\mathbf{v}(\mathbf{p}, t = 0) = 0, \quad (17)$$

$$T(\mathbf{p}, t = 0) = T_0, \quad (18)$$

$$C(\mathbf{p}, t = 0) = C_0, \quad (19)$$

where  $\Omega_H$  and  $\Omega_w$  stand for the rectangle height and width, respectively.

There are at least three reasons why this system is complex to solve. The first complexity is in the presence of strong couplings of heat, mass and momentum transport, and across the scales between the microscopic and macroscopic transport. The second complexity lies in the fact that some of the transport equations are difficult to solve numerically with good accuracy. Finally, the third source of complexity is related to the flow of the liquid metal.

We could basically decompose the couplings into three coupling “loops”. The *first coupling* concerns the hydrodynamic drag force, which acts as a retarding force on the flow in the porous mushy zone (third term on the right-hand side of eq. (2)). Within the mushy zone the drag force varies by several orders of magnitude and depends strongly on the local liquid fraction (the dependence of the permeability on the liquid fraction is given by eq.(6)). The liquid fraction in turn depends on the local phase change at the microscopic scale (eqs. (8)-(10)). The phase change dynamics is determined on the one hand by the local heat extraction, governed by the macroscopic heat transfer (eq.(3)), and, on the other hand, by the local composition, governed by the macroscopic solute transport (eq.(4)). Then again, the macroscopic heat and solute transport are influenced by the flow, as the transport of heat is advective-diffusive (eq. (3)) and the transport of solute is entirely advective (eq. (4)). The first coupling circle is

thus closed. The *second coupling* concerns the driving force for the flow. While the strongest retarding force in the mushy zone is the Darcy drag, the strongest driving force is the buoyancy force (eq. (7)). This is included in the second coupling “loop”, where the liquid density, and thus the buoyancy, depends on the temperature and concentration (eq. (8)). In turn, both the heat and the solute transport are governed by the flow. This is basically the classical coupling of thermosolutal (or double-diffusive) natural convection. However, to make the relations between the heat and the mass transfer even more complex, there is the *third coupling*, associated with the phase change dynamics. This keeps the liquid at the thermodynamic equilibrium, and imposes a tight link between the temperature and the liquid concentration (eq. (10)).

The second reason for the complexity of this system is the hyperbolic nature of the solute transport (eq. (4)) in the fully liquid zone – the solute diffusion on the macroscopic scale is so small that it can be neglected, which makes the solute transfer a completely advective problem. This class of transport problems is difficult to solve numerically with high accuracy. In the mushy zone the equation is nominally not hyperbolic, since the variables in the transient term (average concentration –  $C$ ) and in the advective term (liquid concentration –  $C_L$ ) are not the same and the liquid concentration is also coupled with the temperature. However, the equation remains completely advective.

Finally, the third source of complexity is the potential instabilities that can occur in the thermal and thermosolutal natural convection in liquid metals, due to their low Prandtl number ([Založnik, Xin and Šarler, (2005); Vertnik, Založnik and Šarler, (2006)]). Complex flow patterns and fast transients can occur already in laminar regimes at relatively low Rayleigh numbers. Speaking more mathematically, the low Prandtl number increases the nonlinearity of the natural convection.

A case similar to the Hebditch and Hunt experiment [Hebditch and Hunt, (1974)] and to the SMACS benchmark [Bellet, Combeau, Fautrelle, Gobin, Rady, Arquis, Budenkova, Dussoubs, Duterrail, Kumar, Gandin, Goyeau, Mosbah and Založnik, (2009)] is considered for the numerical tests in the present paper. We are considering a binary Al-4.5%Cu alloy solidifying in a mold of the size of 2×2 cm. Heat is extracted from both vertical walls, while the horizontal walls are insulated. We consider that the problem is two-dimensional. Due to the symmetry only one half of the domain is computed with symmetry boundary conditions applied on the symmetry line (Figure 1), which is the West boundary of the computational domain.

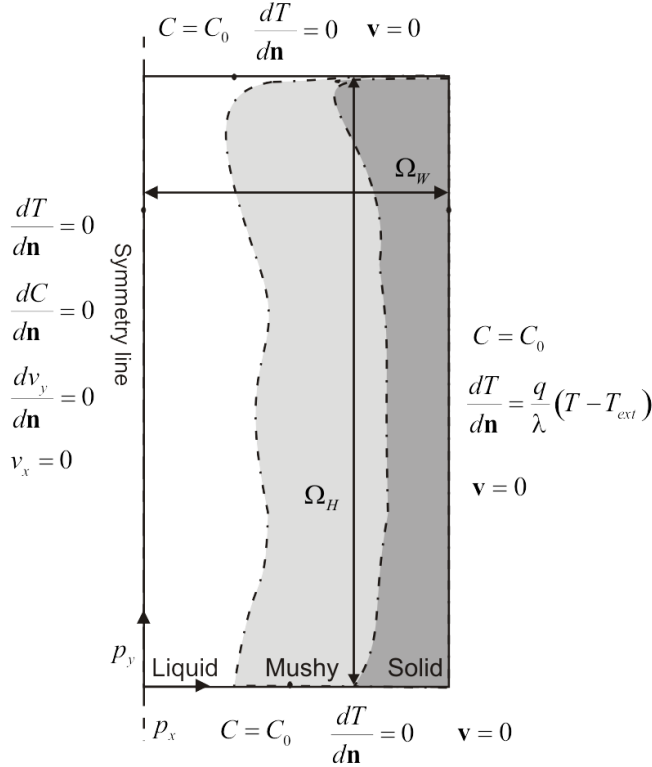


**Figure 1:** The binary alloy solidification benchmark test schematics.

The problem is described in 2-dimensional Cartesian coordinates, i.e.  $\mathbf{p} = p_x \mathbf{i}_x + p_y \mathbf{i}_y$ ,  $\mathbf{v} = v_x \mathbf{i}_x + v_y \mathbf{i}_y$  with  $p_x$  and  $p_y$  standing for Cartesian coordinates and  $v_x$  and  $v_y$  for velocity components.  $\mathbf{i}_x$  and  $\mathbf{i}_y$  denote the base vectors.

The problem is defined with the following initial conditions  $T_0 = 700^\circ\text{C}$ ,  $f_{L0} = 1$ ,  $\mathbf{v}_0 = 0$  m/s,  $C_0 = 4.5\%$ . The North, and South boundaries are of the Neumann insulations type and the West boundary is of the Neumann type as well, due to the symmetry considerations. The East boundary is of the Robin type with the heat transfer coefficient  $q = 500$  W/m<sup>2</sup> K, and the reference temperature  $T_{ext} = 20^\circ\text{C}$ . The velocity on the entire boundary is set to zero, except on the West boundary, where the symmetry is considered and therefore the vertical velocity normal gradient is zero. Instead of setting the concentration gradient on the entire boundary to zero as required in convective-diffusive problems, we set the concentration on the entire boundary to the initial concentration  $C_0$  (again the West boundary is of Neumann type due to the symmetry). The reason is that in the present case we have only the convective transport ( $D = 0$  m<sup>2</sup>/s) and the a priori known exact solution of the solute transport problem at the walls (where the velocity is of the non-slip type) reduces Eq. (4) to

$$\frac{\partial C}{\partial t} = 0; \mathbf{p} \in \Gamma. \quad (20)$$

The absence of the diffusion term in the species transfer equation implies the following: (I) the adjacent Dirichlet boundary condition (used in the present work) does not influence the solution in the interior of the domain (also when valued different from  $C_0$ ), (II) insulation boundary condition  $\partial C / \partial \mathbf{n} = 0$  could not be applied since it can produce considerable errors due to the lack of the diffusion.

**Table 1:** Thermophysical parameters

Density	$\rho$	2.45e+03	kg/m <sup>3</sup>
Specific heat	$c_p$	1.00e+03	J/kgK
Thermal conductivity	$\lambda$	1.92e+02	W/mK
Latent heat of pure Al	$L$	4.00e+05	J/kg
Liquid dynamic viscosity	$\mu$	1.20e-03	m <sup>2</sup> /s
Thermal expansion coefficient	$\beta_T$	-1.30e-04	K <sup>-1</sup>
Solutal expansion coefficient	$\beta_C$	7.30e-03	% <sup>-1</sup>
Reference temperature	$T_{ref}$	4.65e+02	°C
Reference concentration	$C_{ref}$	4.50e+00	%
Reference density	$\rho_{ref}$	2.50e+03	kg/m <sup>3</sup>
Gravity acceleration $\mathbf{g} = g_y \mathbf{i}_y$	$g_y$	-9.80e+00	m/s <sup>2</sup>
Permeability constant	$K_0$	5.56e-11	m <sup>2</sup>
Pure Al melting temperature	$T_f$	6.60e+02	°C
Al-Cu eutectic temperature	$T_e$	5.48e+02	°C
Eutectic concentration	$C_e$	3.26e+01	%
Cu solubility in Al at eutectic temperature	$C_{es}$	5.63e+00	%
Liquidus slope	$m_L$	-3.43e+00	°C/%
Partition coefficient	$k_p$	1.73e-01	

### 3 Solution procedure

Two completely different numerical approaches are used. The first approach is based on meshless spatial discretization and explicit Euler time stepping and a local pressure correction algorithm [Kosec and Šarler, (2008a)] for pressure-velocity coupling, while the second approach uses the finite-volume spatial discretization, implicit Euler time stepping and the SIMPLE pressure correction algorithm [Založnik and Šarler, (2005)].

#### 3.1 Local radial basis collocation method based approach

The LRBFCM, combined with the local pressure-correction and explicit time discretization, enables the consideration of each computational node separately from other parts of computational domain. Such an approach has already been successfully applied to several thermo-fluid problems [Kosec and Šarler, (2008d); Kosec and Šarler, (2008c); Kosec and

Šarler, (2008b); Kosec and Šarler, (2008a); Kosec and Šarler, (2009)] and it shows several advantages like ease of implementation, straightforward parallelization, simple consideration of complex physical models and CPU effectiveness.

An Euler explicit time stepping scheme is used for time discretization and the spatial discretization is performed by the local meshless method. The general idea behind the local meshless numerical approach is the use of a local influence domain for the approximation of an arbitrary field in order to evaluate the differential operators needed to solve the partial differential equations. The principle is represented in Figure 2.

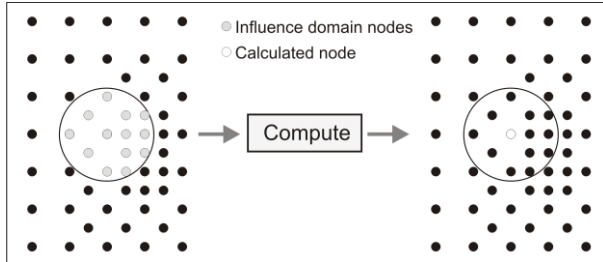


**Figure 2:** Scheme of the influence domain schematics and node in which the solution is sought in a local meshless method.

Each node uses its own support domain for spatial differential operations; the domain is therefore discretized with overlapping support domains. The approximation function is introduced as

$$\theta(\mathbf{p}) = \sum_{n=1}^{N_{Basis}} \alpha_n \Psi_n(\mathbf{p}), \quad (21)$$

where  $\theta$ ,  $N_{Basis}$ ,  $\alpha_n$  and  $\Psi_n$  stand for the interpolation function, the number of basis functions, the approximation coefficients and the basis functions, respectively. The basis could be selected arbitrarily, however in this paper only Hardy's Multiquadrics (MQs)

$$\Psi_n(\mathbf{p}) = \sqrt{(\mathbf{p} - \mathbf{p}^n) \cdot (\mathbf{p} - \mathbf{p}^n) / \sigma_c^2 + 1}, \quad (22)$$

with  $\sigma_c$  standing for the free shape parameter of the basis function, are used. By taking into account all support domain nodes and equation (21), the approximation system is obtained. In this paper the simplest possible case is considered, where the number of support domain nodes is exactly the same as the number of basis functions. In such a case the approximation simplifies to collocation. With the constructed collocation function an arbitrary spatial differential operator ( $L$ ) can be computed

$$L\theta(\mathbf{p}) = \sum_{n=1}^{N_{Basis}} \alpha_n L\Psi_n(\mathbf{p}). \quad (23)$$

In this work only five-node support domains are used and therefore a basis of five MQs is used as well.

The implementation of the Dirichlet boundary condition is straightforward. In order to implement Neumann and Robin boundary conditions, however, a special case of interpolation is needed. In these boundary nodes the function directional derivative instead of the function value is known and therefore the equation in the interpolation system changes to

$$\theta_{BC} = \sum_{n=1}^{N_{Basis}} \alpha_n \frac{\partial}{\partial \mathbf{n}} \Psi_n(\mathbf{p}), \quad (24)$$

in the Neumann boundary nodes and to

$$\theta_{BC} = \sum_{n=1}^{N_{Basis}} \alpha_n \left( a \frac{\partial}{\partial \mathbf{n}} \Psi_n(\mathbf{p}) + b \Psi_n(\mathbf{p}) \right), \quad (25)$$

in the Robin boundary nodes.

With the defined time and spatial discretization schemes, the general transport equation can under the model assumptions be written as

$$\rho_0 \frac{\theta - \theta_0}{\Delta t} = \nabla \cdot (D_0 \nabla \theta_0) - \nabla \cdot (\rho_0 \mathbf{v}_0 \theta_0) + S_0 \quad (26)$$

Where zero-indexed quantities stand for the values at the initial time, and  $D$ ,  $S$  for general diffusion coefficient, and source term, respectively.

To couple the mass and momentum conservation, a special treatment is required. The intermediate velocity  $\hat{\mathbf{v}}$  is computed

$$\hat{\mathbf{v}} = \mathbf{v}_0 + \frac{\Delta t}{\rho} (-\nabla P_0 + \nabla \cdot (\mu \nabla \mathbf{v}_0) + \mathbf{b}_0 - \nabla \cdot (\rho \mathbf{v}_0 \mathbf{v}_0)) \quad (27)$$

The equation (27) did not take into account the mass continuity and so the pressure and the velocity corrections are added to correct it

$$\hat{\mathbf{v}}^{m+1} = \hat{\mathbf{v}}^m + \hat{\mathbf{v}}, \quad \hat{P}^{m+1} = \hat{P}^m + \hat{P}, \quad (28)$$

where  $m$ ,  $\hat{\mathbf{v}}$  and  $\hat{P}$  stand for pressure velocity iteration index, velocity correction and pressure correction, respectively. By combining the momentum and the mass continuity equations the pressure correction Poisson equation emerges

$$\nabla \cdot \hat{\mathbf{v}}^m = \frac{\Delta t}{\rho} \nabla^2 \hat{P}. \quad (29)$$

Instead of solving the global Poisson equation problem, the pressure correction is directly related to the divergence of the intermediate velocity.

$$\hat{P} = \ell^2 \frac{\rho}{\Delta t} \nabla \cdot \hat{\mathbf{v}}^m. \quad (30)$$

The proposed assumption enables direct solving of the pressure velocity coupling iteration and thus is very fast, since there is only one step needed in each node to evaluate the new iteration pressure and the velocity correction. With the

computed pressure correction the pressure and the velocity can be corrected as

$$\hat{\mathbf{v}}^{m+1} = \hat{\mathbf{v}}^m - \zeta \frac{\Delta t}{\rho} \nabla \hat{P} \quad \hat{P}^{m+1} = \hat{P}^m + \zeta \hat{P}, \quad (31)$$

where  $\zeta$  stands for relaxation parameter. The iteration is performed until the criterion  $\nabla \cdot \hat{\mathbf{v}} < \varepsilon_v$  is met in all computational nodes.

The radial basis function shape parameter has been set to  $\sigma_c = 90$  for all computations. The value of shape parameter has been determined by analysis of the interpolation system condition number (eq. (21)). It has been shown that using more sensitive interpolation system results in better accuracy of the method. This phenomenon has been reported in numerical observations [Lee, Liu and Fan, (2003); Kosec and Šarler, (2008a)] and theoretical work [Schaback, (1995)], as well. Schaback [Schaback, (1995)] showed the uncertainty relation between attainable error and the condition number of the interpolation matrix. However, the condition number of the interpolation matrix should be kept below critical value, where the system becomes ill-conditioned. However, the selection of  $\sigma_c = 90$  stands for optimal choice regarding the accuracy and stability. The time step is set to  $\Delta t = 10^{-5}$  s for computations on node distributions up to 10011 nodes (71x141) and  $\Delta t = 0.5 \cdot 10^{-5}$  s for computations on finer node distributions (up to 29161 nodes for the 121x241 distribution). Numerical value of the pressure velocity coupling relaxation parameter has been set to  $\zeta = 10^{-3} \Delta t$  for all computations. Computations have been performed on the uniform node distributions of 21x41, 51x101, 71x141, 101x201 and 121x241 nodes, where the four corner nodes have not been considered.

### 3.2 The FVM solution

The finite volume code used for the computations follows a more conventional approach. It implements a QUICK (quadratic upwind-oriented) interpolation for convection in all equations except in the energy equation, where we used the linear interpolation scheme, and a second-order centred scheme for diffusion. This treatment makes the discretization theoretically second-order accurate overall (contrarily to first-order discretization schemes, still widely used in codes for solution of this kind of solidification problems). The resolution of the velocity-pressure coupling is performed by the SIMPLE (semi-implicit method for pressure-linked equations) algorithm, on a collocated pressure-velocity arrangement, using the Rhie-Chow momentum interpolation. For integration in time, implicit Euler (first order) timestepping is used. The approach has been already successfully used in [Založnik and Šarler, (2005); Založnik, Xin and Šarler, (2005)].

Computations have been performed on grids of 21x41, 51x101, 71x141, 101x201 and 121x241. These include normal interior control volumes and additional nodes (with zero volume) on the boundary. A time step of  $\Delta t = 10^{-4}$  s was used in all computations.

### 3.3 Solution of phase change and micro-macro coupling

Our description of solidification requires the coupling of phenomena that occur on two different length scales. On the one hand the macroscopic transport of heat, momentum and solute is described by transport equations, which give the variation of enthalpy (eq. (3)), pressure and velocity (eq. (5) and (2)), and average concentration (eq. (4)). The additional variables needed to solve the system (liquid fraction –  $f_L$ , liquid concentration –  $C_L$  and temperature –  $T$ ) are determined by the phase change phenomena occurring at the microscopic scale. In the present “minimal” solidification model these are obtained assuming full thermodynamic equilibrium locally, which is represented by eq. (8)-(10). By substitution (eq. (8)-(10)) are combined into a quadratic equation, which is solved analytically for the liquid fraction  $f_L$

$$\begin{aligned} af_L^2 + bf_L + c &= 0, \\ a &= (k_p - 1)L, \\ b &= (k_p - 1)(c_p T_f - h) - k_p L, \\ c &= k_p (h - c_p T_F) - c_p m_L C_L. \end{aligned} \quad (32)$$

The liquid concentration  $C_L$  and temperature  $T$  are then computed by substituting  $f_L$  into eq. (10) and (8). This approach was already described in [Založnik and Šarler, (2005)].

### 3.4 The solution procedure overview

The local meshfree approach can be summarized in the following steps:

- (1) Solve the velocity (eq. (5)) from previous time step values.
- (2) Force the velocity to a divergence-free field with the presented local pressure-velocity coupling algorithm (eq. (31)).
- (3) Solve energy and solute transport equations using the velocity, liquid fraction, concentration and temperature from previous time step.
- (4) Solve the local phase change (eq. (8)-(10)) by the aforementioned procedure and obtain the new liquid fraction,
- (5) Update all variables and proceed to the next time step

In the finite volume code the coupling is done by the following iterative procedure:

(1) Solve the velocity and pressure (eq. (5) and (2)) in a SIMPLE step using the liquid fraction, concentration and temperature from the previous iteration.

(2) Solve the enthalpy and concentration using the new velocity, and the liquid fraction, concentration and temperature from the previous iteration.

(3) Solve the local phase change (eq. (8)-(10)) by the aforementioned procedure and obtain the new liquid fraction, liquid concentration and temperature.

(4) Steps 1–3 are iterated until convergence, and then the algorithm advances to a new time step.

## 4 Results

### 4.1 The solidification process

Before presenting the comparison of the results, we will show the evolution of the solidification. Figure 5 and Figure 6 show the temperature field, the streamlines, and the liquid fraction and solute concentration fields during solidification at  $t = 5$  s,  $t = 10$  s and after completed solidification at  $t = 50$  s. The liquid metal is initially superheated by about 55 K ( $T_0 - T_{LQ} = 55.508$  K) ( $T_{LQ}$  stands for liquidus temperature). When it starts to cool down, a natural convection is set up, reaching an effective Rayleigh number of  $\sim 2500$  and velocities of the order of  $\sim 1$  cm/s at times between 3 s and 4 s. As the initial superheat of the bulk liquid zone is gradually extracted, the thermal natural convection flow calms down. At the right wall solidification starts a bit before  $t = 4$  s, and the whole superheat from the bulk liquid (up to the left wall) is extracted at about  $t = 5$  s. We can see that the main features of the macrosegregation develop early through the solidification process. After about  $t \sim 10$  s the principal characteristics can be recognized: a positive segregation patch at the bottom of the enclosure and a negative segregation zone in the central upper part. This pattern is easily explained by combining eq. (3) and eq. (4). We obtain

$$\frac{\partial C}{\partial t} = -\frac{1}{m_L} \mathbf{v} \cdot \nabla T, \quad (33)$$

which shows that the segregation tendency depends on the direction of the flow with respect to the isotherms (note that  $m_L < 0$ ). The solidification, and thus the advancement of the mushy zone, is retarded at the bottom due to local enrichment, and accelerated at the top due to local depletion in solute. The time evolution of the average concentration versus the liquid fraction in the four test points, shown in Figure 4, shows that the macrosegregation continues to evolve down to liquid fractions of  $f_L \approx 0.4$  (this limiting value of course depends of the permeability constant  $K_0$ ). The segregation field stays relatively smooth, there is no destabilisation of the mushy zone and channel mesosegregates do not develop.

The numerical solution is presented in terms of temperature and concentration contour plots, streamlines, concentration cross sections, time evolutions of liquid fraction, concentration, velocity and temperature, and grid convergence analysis. In Figure 3 the sampling points and cross sections are presented.

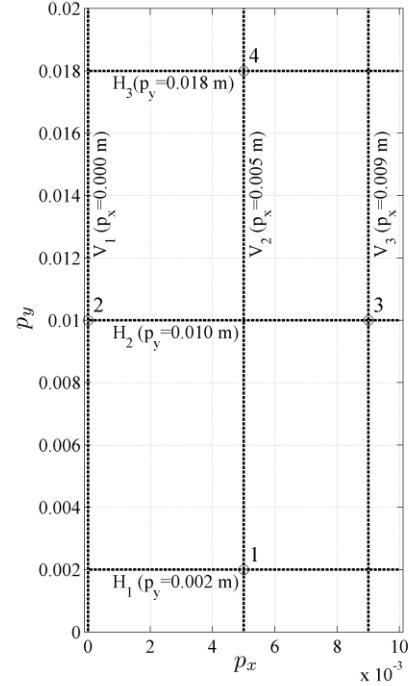


Figure 3: Sampling points and cross section lines.

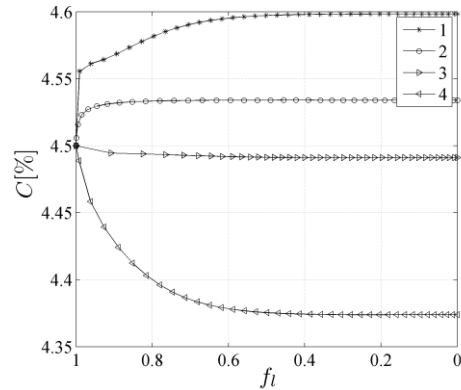
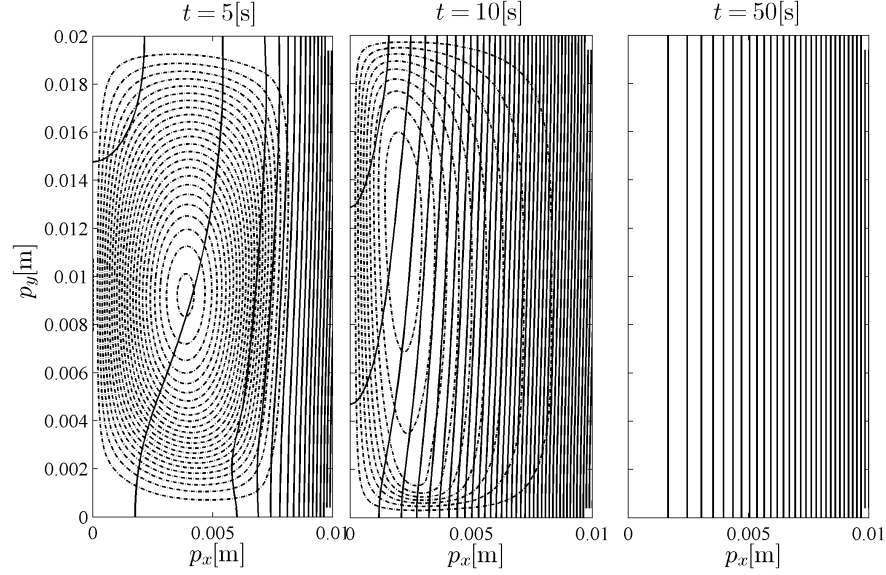
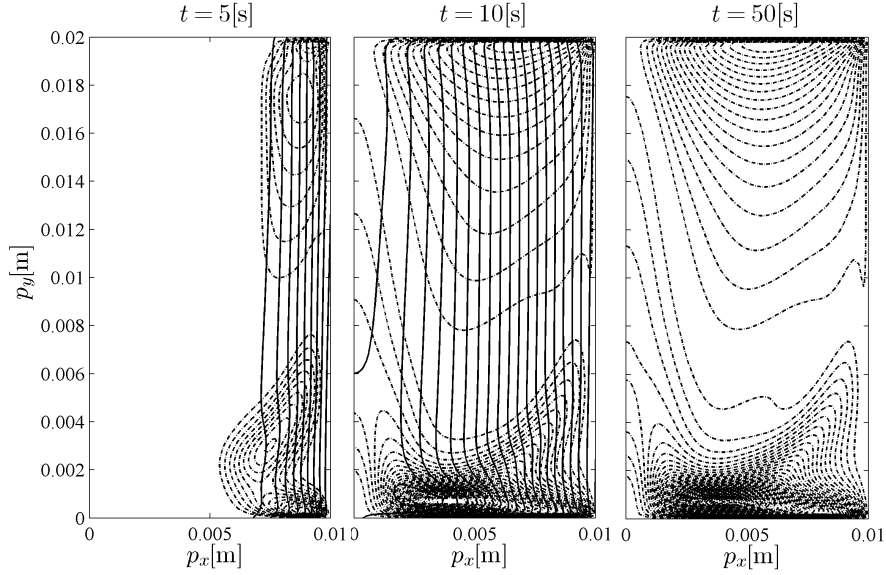


Figure 4: Evolutions of the average concentration versus liquid fraction in the four sampling points.



**Figure 5:** Temperature (solid) and streamlines (dashed) contour plots at  $t=5$  s,  $t=10$  s and  $t=50$  s with a temperature contour step of 0.25 K and a streamline contour step of  $1e-4$  m<sup>2</sup>/s at  $t=5$  s and  $5e-6$  m<sup>2</sup>/s at  $t=10$  s. At  $t=50$  s a fully solidified state is depicted (note the absence of the streamline contours).



**Figure 6:** Liquid fraction (solid) and concentration (dashed) contour plots at  $t=5$  s,  $t=10$  s and  $t=50$  s. The concentration and liquid fraction contour steps are 0.01% and 0.02, respectively. At  $t=50$  s a fully solidified state is depicted (note the absence of the liquid fraction contours).

## 4.2 Comparison and analysis of the numerical results

The results of numerical integration are presented in Figures 5-9, which are representative for all the computations that were done on several grids, since the differences are rather small. For more detailed demonstrations we show the comparisons between the finite-volume and the meshless results in Figures 7-10. In Figure 7 and Figure 8 time evolutions of liquid fraction, concentration, velocity and temperature in four sampling points are shown. In Figure 9 we compare profiles of the final concentration field along three horizontal and three vertical cross-sections. An additional numerical comparison of these profiles is presented in Tables 2 and 3. These comparisons are done on results computed with the finest spatial discretization of 29161 uniformly distributed nodes (grid 121x241).

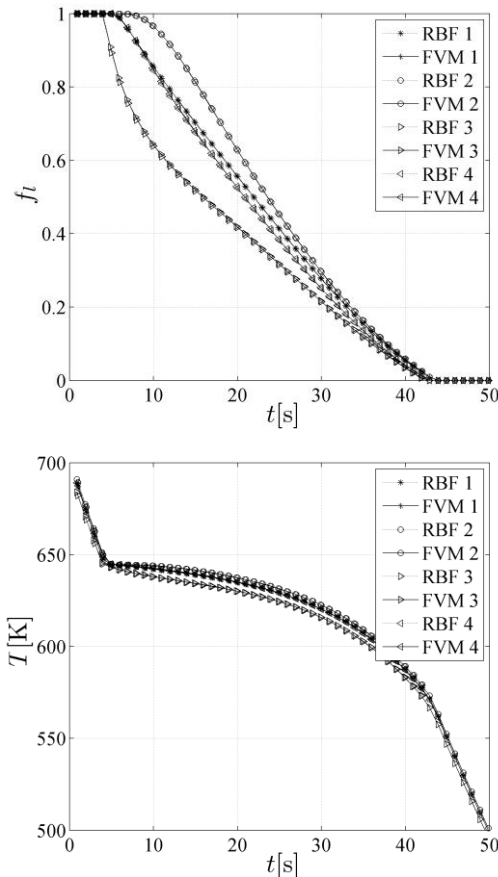


**Figure 7:** Evolution of the liquid fraction, temperature in the four sampling points (See Fig. 3 right) as calculated by the LRBFCM and FVM methods.

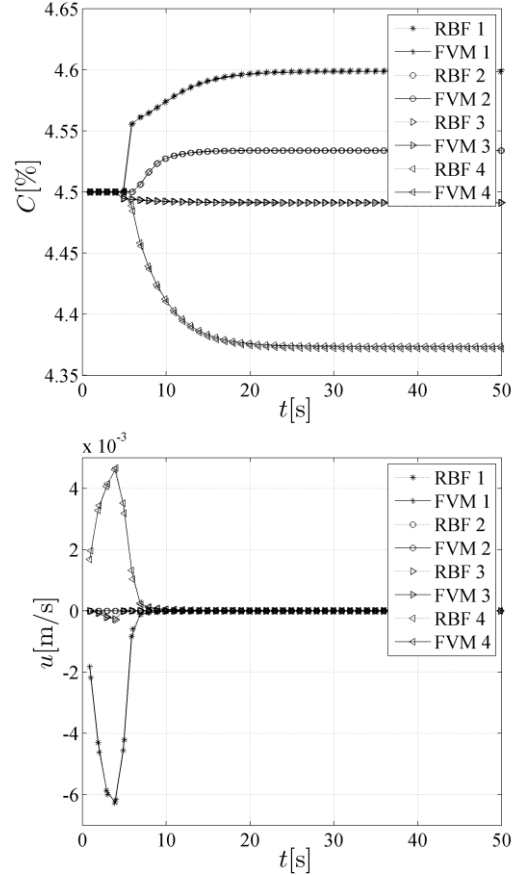


**Figure 8:** Evolution of the concentration and velocity during solidification in the four sampling points (See Fig. 3 right) as calculated by the LRBFCM and FVM methods.

**Table 2:** The LRBFCM and FVM computed vertical cross sections.

	V1		V2		V3	
$p_y$	$C_{\text{RBF}}$	$C_{\text{FVM}}$	$C_{\text{RBF}}$	$C_{\text{FVM}}$	$C_{\text{RBF}}$	$C_{\text{FVM}}$
0	4,5	4,5	4,5	4,5	4,5	4,5
0,002	4,5125	4,5127	4,5982	4,6018	4,5279	4,5276
0,004	4,5327	4,5332	4,5144	4,5149	4,5311	4,5298
0,006	4,5402	4,5405	4,5026	4,5028	4,5266	4,5260
0,008	4,5390	4,539	4,4895	4,4894	4,5033	4,5034
0,01	4,5340	4,5337	4,4775	4,4771	4,4911	4,4913
0,012	4,5279	4,5278	4,4650	4,465	4,4815	4,4822
0,014	4,5224	4,5221	4,4495	4,4494	4,4702	4,4709
0,016	4,5166	4,5162	4,4229	4,4225	4,4540	4,4548
0,018	4,5074	4,5069	4,3737	4,3725	4,4332	4,4339
0,02	4,5	4,5	4,5	4,5	4,5	4,5

**Table 3:** The LRBFCM and FVM computed horizontal cross sections.

	H1		H2		H3	
$p_x$	$C_{\text{RBF}}$	$C_{\text{FVM}}$	$C_{\text{RBF}}$	$C_{\text{FVM}}$	$C_{\text{RBF}}$	$C_{\text{FVM}}$
0	4,5125	4,5127	4,5340	4,5337	4,5074	4,5069
0,001	4,5569	4,5557	4,5245	4,5246	4,4887	4,4889
0,002	4,6040	4,6059	4,5060	4,5059	4,4490	4,4484
0,003	4,5791	4,5805	4,4909	4,4906	4,4122	4,4108
0,004	4,5744	4,5764	4,4813	4,4809	4,3868	4,3852
0,005	4,5982	4,6018	4,4775	4,4771	4,3737	4,3725
0,006	4,6382	4,6398	4,4794	4,4789	4,3730	4,3720
0,007	4,6282	4,6287	4,4835	4,4833	4,3833	4,3825
0,008	4,5717	4,5715	4,4863	4,4863	4,4030	4,4071
0,009	4,5279	4,5276	4,4911	4,4913	4,4332	4,4339
0,01	4,5	4,5	4,5	4,5	4,5	4,5

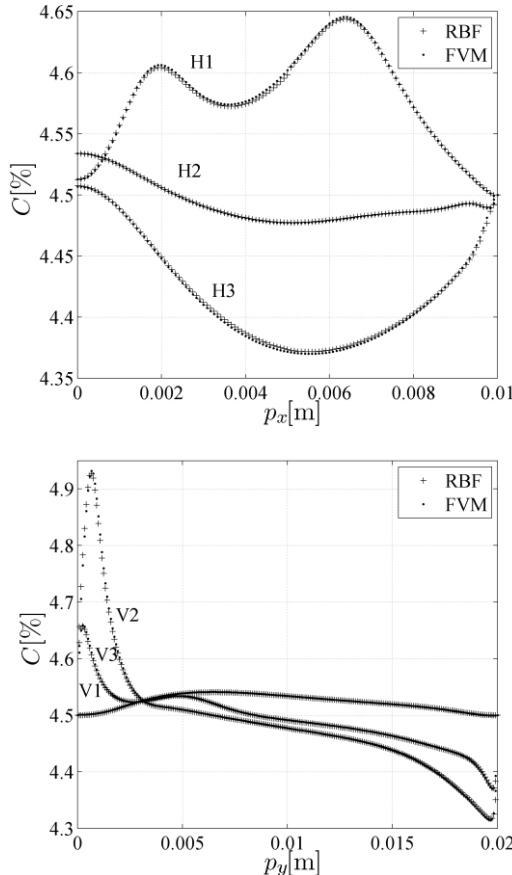


**Figure 9:** Horizontal and vertical cross-sections of the final concentration.

As we can see, the differences between the solutions by the two methods become extremely small at fine grids. Therefore we investigated the behavior of the solutions during grid re-

finement from the very coarse 21x41 to the fine 121x241 grid. We analyzed the convergence of representative characteristics of the final segregation field. The final segregation field is at the same time the result upon which our interest is focused, and is also the most sensitive quantity. The whole evolution of the solution, from the onset until the completion of the solidification, is reflected in the final concentration field in the domain. We looked closer at the convergence of the maximum value of the macrosegregation in the domain

$$C^{\max} = \max(C - C_0), \quad (34)$$

and of the standard deviation of the concentration  $\sigma_c$ , sometimes also called “global segregation index”, defined as

$$\sigma_c = \sqrt{\frac{1}{N} \sum_{i=1}^N (C(\mathbf{p}_i) - C_0)^2}. \quad (35)$$

In the computation of  $\sigma_c$  for the LRBFCM method, all computational nodes have been included, while in the FVM method, the boundary nodes have been excluded, since they correspond to finite volumes with a zero volume and can therefore not contribute to the variance of the field. Let us recall that the node distributions in the LRBFCM computations and the volume sizes in the FVM computations are uniform.

Figure 10 shows the grid convergence of the final segregation field in terms of these two functionals. Both show convergent behavior. We can also see that the maximum concentration reaches the convergent regime sooner than the standard deviation of the macrosegregation field. Both solutions behave strikingly similar with respect to the maximum segregation, although a shift between them persists, but becomes smaller with finer grids. The standard deviation appears to converge faster with the LRBFCM method, but the method shows larger errors than the FVM at coarse node arrangements. Looking into more detail at the convergence shown in Figure 10, we can see that the relative differences between the results on the densest grids are of the order of  $10^{-3}$  for both methods. Despite that, the difference between the two methods remains larger, of the order of  $10^{-2}$  even on dense grids. It is not entirely clear to what asymptotical values the solutions should converge as the grid distance  $\Delta x$  approaches zero. It is also not obvious whether the two methods converge towards the same asymptotical solution or how large their difference is. However, if we imagine an extrapolation of the convergence plots to  $\Delta x = 0$ , we could estimate the errors as well as the differences between the two extrapolated solutions to be within a relative band of  $10^{-2}$ . We do not show the extrapolations in the plots, since we believe that it was not possible to perform them unambiguously and to sufficient precision with the present results. A possible source of error that could become important at dense grids, when the spatial discretization errors decrease, is the error of the temporal discretization, which should be ordered in the timestep. Note

that both methods used a first-order time integration scheme. However the time steps used were different. A timestep of  $10^{-4}$  s was used for the FVM solutions with a time-implicit algorithm. For the LRBFCM solution much smaller timesteps ( $10^{-5}$  s for the coarse grids and  $5 \times 10^{-6}$  s for the two densest grids) were used due to stability limitations of the time-explicit algorithm, as well as stability issues due to the local pressure-velocity coupling. The dependence on the timestep appears to be an important property of the solution of macrosegregation, which should be investigated in the future. However, in the present paper it is not our goal to characterize the grid convergence in detail or to perform an extrapolation to estimate an exact solution.

Our most important conclusion from the convergence study is that the observed grid convergence behavior of both solutions is fundamentally different from previously studied solutions, which included mesosegregations [Kumar, Dussoubs, Založnik and Combeau, (2009); Combeau, Bellet, Fautrelle, Gobin, Arquis, Budenkova, Dussoubs, Duterrail, Kumar, Goyeau, Mosba, Quatruvaux, Rady, Gandin and Založnik, (2011)]. In solutions with mesosegregations the convergence was often observed to slow down considerably at dense grids. The most probable reason for this seemed to be that at finer grids the solutions started to capture fine-scale (mesoscopic) features of the solution fields (such as flow in the remelted channels), which the coarser grids did not adequately describe. In the present case the solution appears to be smooth and the grid convergence is therefore simpler to investigate. Nevertheless, the couplings and the nonlinearities of the problem remain strong. It is not easy to obtain a highly precise solution and dense node distributions are needed. Therefore the presented case can be a suitable benchmark test case for rigorous testing of numerical codes dedicated to the simulation of macrosegregation, an alternative or a preliminary to the physically and numerically more complex cases proposed in [Bellet, Combeau, Fautrelle, Gobin, Rady, Arquis, Budenkova, Dussoubs, Duterrail, Kumar, Gandin, Goyeau, Mosbah and Založnik, (2009)]. The convergence behavior of both applied methods also indicates that it should be possible to obtain a highly precise reference solution of this case. This will require a more extensive convergence study with respect to grid distance and timestep and detailed error estimation.

We used the proposed case to demonstrate the first application of a meshless method for the solution of the macrosegregation problem. In first comparisons we can observe that it behaves comparably to a classical, nominally second-order accurate finite-volume method. Both numerical approaches give very close predictions even for such a highly nonlinear problem. Let us point out that the proposed novel meshless approach is one of the simplest possible. It employs an entirely local solution procedure, using local pressure-velocity coupling and explicit timestepping. Thanks to this it shows

several convenient properties like straightforward implementation and parallelization, CPU effectiveness and several degrees of freedom for optimization, which makes the method flexible.

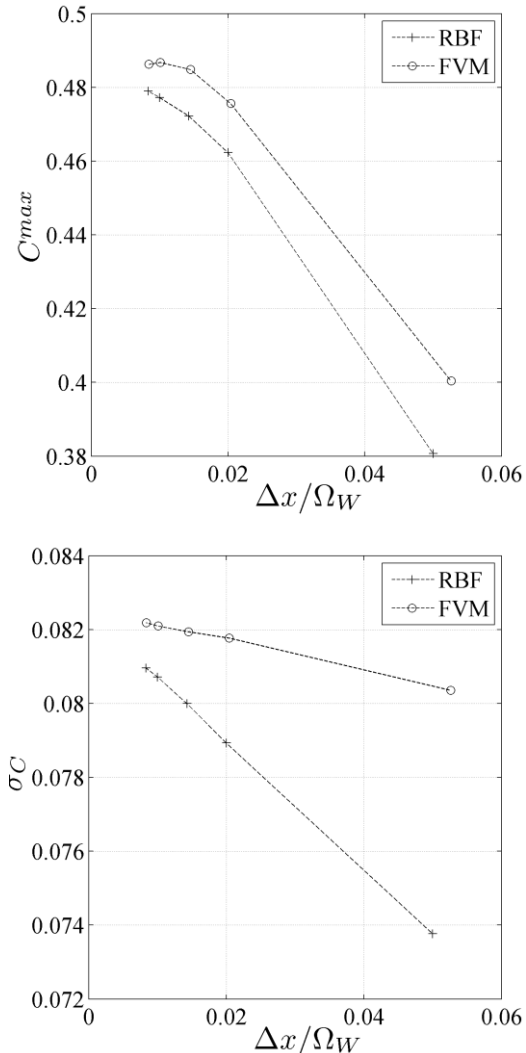


Figure 10: Convergence plots.

## 5 Conclusions and perspectives

The present paper deals with the simulation of macrosegregation. Two completely different numerical approaches are used in order to predict phenomena during the solidification of a binary alloy in order to confirm correct behavior of numerical solution. The classical FVM based solution procedure with SIMPLE pressure-velocity coupling and implicit time stepping is compared against and a completely local meshless based solution procedure with local pressure-velocity coupling and explicit time stepping.

The evaluation of the results has been performed by comparing computations done by both numerical methods on several different node distribution densities. It has been shown that both numerical approaches perform similar in terms of the quantitative results and the grid convergence. The solution thus properly depicts the posed minimal solidification system and gives us an insight and improved understanding of the respective system dynamics. It has been shown in the paper that it is possible to get consistent results of this highly non-linear and coupled problem. However, it is still an open question if a similar sharp focus of the prediction can be achieved also in case of the presence of the mesoscopic instabilities.

The second focus of the present work is on the meshless method itself, as it is for the first time used in such problems. The proposed novel meshless method shows several convenient properties like straightforward implementation and parallelization suitability, CPU effectiveness and several degrees of freedom for optimization, which makes the method flexible. The flexible point adaptivity strategy [Kosec and Šarler, (2010)] makes it a promising alternative even for more complex problems of the same kind (mesoscopic instabilities). The solution of these, even more difficult problems, is in the focus of our future research, together with coupling of the macro-mesoscopic predictions with the cellular automata based grain structure evolution. A compatible meshless strategy, relying on points instead of polygons has been developed very recently [Lorbiecka and Šarler, (2010)].

## 6 Acknowledgment

The authors would like to express their gratitude to Slovenian Research Agency for support in the framework of the projects Young Researcher Programme 1000-06-310232, project J2-0099 Multiscale Modelling and Simulation of Liquid-Solid Systems, and programme group P2-0379 Modelling and Simulation of Materials and Processes. The collaboration of the French and Slovenian-French project groups was supported by the Slovenian Research Agency and by Égide via the PHC-Proteus 2009-2010: Advanced Modelling of Solidification: Development of Reference Tests and Numerical Methods programme.

## 7 References

Ahmad, N.; Combeau, H.; Desbiolles, J. L.; Jalanti, T.; Lesoult, G.; Rappaz, J.; Rappaz, M.; Stomp, C. (1998): Numerical simulation of macrosegregation: a comparison between finite volume method and finite element method predictions and a confrontation with experiments. *Metallurgical and Materials Transactions*, vol. A29, pp. 617.

Bellet, M.; Combeau, H.; Fautrelle, Y.; Gobin, D.; Rady, M.; Arquis, E.; Budenkova, O.; Dussoubs, B.; Duterrail, Y.; Kumar, A.; Gandin, C. A.; Goyeau, B.; Mosbah, S.; Založnik, M. (2009): Call for contributions to a numerical

benchmark problem for 2D columnar solidification of binary alloys. *International Journal of Thermal Sciences*, vol. 48, pp. 2013-2016.

Buhmann, M. D. (2000): *Radial Basis Functions*, Cambridge University Press, Cambridge.

Cockcroft, L. S.; Maijer, D. M. (2009): *Modeling of Casting, Welding, and Advanced Solidification Processes XII*, The Minerals, Metals & Materials Society, Warrendale.

Combeau, H.; Bellet, M.; Fautrelle, Y.; Gobin, D.; Arquis, E.; Budenkova, O.; Dussoubs, B.; Duterrail, Y.; Kumar, A.; Goyeau, B.; Mosba, S.; Quatravaux, T.; Rady, M. A.; Gandin, C. A.; Založnik, M. (2011): A Numerical Benchmark on the Prediction of Macrosegregation in Binary Alloys, *Frontiers in Solidification Science*.

Combeau, H.; Založnik, M.; Hans, S.; Richy, P.E. (2009): Prediction of Macrosegregation in Steel Ingots: Influence of the Motion and the Morphology of Equiaxed Grains. *Metallurgical and Materials Transactions*, vol. B40, pp. 289-304.

Drew, D. A. (1983): Mathematical modeling of two-phase flow. *Annual Review of Fluid Mechanics*, vol. 15, pp. 261-291.

Flemings, M. C.; Nereo, G. E. (1967a): Macrosegregation, part I. *Transactions of Society for Metals AIME*, vol. 239, pp. 1449-1461.

Flemings, M. C.; Nereo, G. E. (1967b): Macrosegregation, part II. *Transactions of Society for Metals AIME*, vol. 242, pp. 50-55.

Flemings, M. C. (1974): Solidification Processing. *Metallurgical and Materials Transactions* vol. B5, pp. 2121-2134.

Ganesan, S.; Poirier, D. (1990): Conservation of mass and momentum for the flow of inter dendritic liquid during solidification. *Metallurgical and Materials Transactions*, vol. B21, pp. 173-181.

Goyeau, B.; Bousquet-Melou, P.; Gobin, D.; Quintard, M.; Fichot, F. (2004): Macroscopic modeling of columnar dendritic solidification. *Computational & Applied Mathematics*, vol. 23, pp. 381-400.

Hebditch, D. J.; Hunt, J. D. (1974): Observations of ingot macrosegregation on model systems. *Metallurgical transactions*, vol. 5, pp. 1557-1564.

Kansa, E. J. (1990a): Multiquadrics - a scattered data approximation scheme with application to computational fluid dynamics, part I. *Computers and Mathematics with Applications*, vol. 19, pp. 127-145.

Kansa, E. J. (1990b): Multiquadrics - a scattered data approximation scheme with application to computational fluid dynamics, part II. *Computers and Mathematics with Applications*, vol. 19, pp. 147-161.

Kosec, G.; Šarler, B. (2008a): Solution of thermo-fluid problems by collocation with local pressure correction. *International Journal of Numerical Methods for Heat and Fluid Flow*, vol. 18, pp. 868-882.

- Kosec, G.; Šarler, B.** (2008b): Local RBF collocation method for Darcy flow. *CMES: Computer Modeling in Engineering & Sciences*, vol. 25, pp. 197-208.
- Kosec, G.; Šarler, B.** (2008c): Convection driven melting of anisotropic metals. *International Journal of Cast Metals Research*, vol. 22, pp. 279-282.
- Kosec, G.; Šarler, B.** (2008d): Meshless approach to solving freezing driven by a natural convection. *Materials Science Forum*, vol. 649, pp. 205-210.
- Kosec, G.; Šarler, B.** (2009): Solution of phase change problems by collocation with local pressure correction. *CMES: Computer Modeling in Engineering & Sciences*, vol. 47, pp. 191-216.
- Kosec, G.; Šarler, B.** (2010): Adaptive meshfree method for thermo-fluid problems with phase change, *Eighth International Conference on Advances in Fluid Mechanics*.
- Kumar, A.; Dussoubs, B.; Založnik, M.; Combeau, H.** (2009): Effect of discretization of permeability term and mesh size on macro- and meso-segregation predictions. *Journal of Physics D: Applied Physics*, vol. 42, pp. 105503.
- Lee, C. K. ; Liu, X.; Fan, S.C.** (2003): Local multiquadric approximation for solving boundary value problems. *Computational Mechanics*, vol. 30, pp. 395-409.
- Lesoult, G.** (2005): Macro-segregation in steel strands and ingots: Characterisation, formation and consequences. *Materials Science and Engineering: A*, vol. 413-414, pp. 19-29.
- Lorbiecka, A. Z.; Šarler, B.** (2010): Simulation of dendritic growth with different orientation by using the point automata method. *CMC*, vol. 18, pp. 69-103.
- Ni, J.; Beckermann, C.** (1991): A volume-averaged two-phase model for transport phenomena during solidification. *Metallurgical and Materials Transactions B*, vol. 22B, pp. 349-361.
- Schaback, R.** (1995): Error estimates and condition numbers for radial basis function interpolation. *Advances in Computational Mathematics*, vol. 3, pp. 251-264.
- Šarler, B.; Vertnik, R.** (2006): Meshfree explicit local radial basis function collocation method for diffusion problems. *Computers and Mathematics with Applications*, vol. 51, pp. 1269-1282.
- Vertnik, R.; Šarler, B.** (2011): Local collocation approach for solving turbulent combined forced and natural convection pro. *Adv. appl. math. mech*, vol. 3, pp. 259-279.
- Vertnik, R.; Šarler, B.** (2006): Meshless local radial basis function collocation method for convective-diffusive solid-liquid phase change problems. *International Journal of Numerical Methods for Heat and Fluid Flow*, vol. 16, pp. 617-640.
- Vertnik, R.; Šarler, B.** (2009): Solution of incompressible turbulent flow by a mesh-free method. *CMES: Computer Modeling in Engineering & Sciences*, vol. 44, pp. 65-95.
- Vertnik, R.; Založnik, M.; Šarler, B.** (2006): Solution of transient direct-chill aluminium billet casting problem with simultaneous material and interphase moving boundaries by a meshless method. *Engineering Analysis with Boundary Elements*, vol. 30, pp. 847-855.
- Voller, V. R.** (2001): On a general back-diffusion parameter. *Journal of Crystal Growth*, vol. 226, pp. 562-568.
- Wang, C. Y. ; Beckermann, C.** (1996a): Equiaxed dendritic solidification with convection: Part I. multiscale/multiphase modeling. *Metallurgical and Materials Transactions*, vol. A27, pp. 2754-2764.
- Wang, C. Y. ; Beckermann, C.** (1996b): Equiaxed dendritic solidification with convection: Part II. numerical simulation for an Al-4 wt pct Cu alloy. *Metallurgical and Materials Transactions*, vol. A27, pp. 2765-2783.
- Založnik, M.; Kumar, A.; Combeau, H.** (2010): An operator splitting scheme for coupling macroscopic transport and grain growth in a two-phase multiscale solidification model: Part II Application of the model. *Computational Materials Science*, vol. 48, pp. 11-21.
- Založnik, M.; Šarler, B.** (2005): Modeling of macrosegregation in direct-chill casting of aluminum alloys: Estimating the influence of casting parameters. *Materials Science and Engineering*, vol. A413-414, pp. 85-91.
- Založnik, M.; Xin, S.; Šarler, B.** (2005): Verification of a numerical model of macrosegregation in direct chill casting. *International Journal of Numerical Methods for Heat & Fluid Flow*, vol. 18, pp. 308-324.